Long-range empirical potential model: Application to fcc transition metals and alloys

X. D. Dai, Y. Kong, and J. H. Li*
Department of Materials Science and Engineering, Tsinghua University, Beijing 100084, China
(Received 10 November 2006; revised manuscript received 15 January 2007; published 5 March 2007)

Under the framework of the second moment approximation of tight-binding theory, a long-range empirical potential (LREP) is developed for transition metals in the present study and successfully applied to Cu, Ag, Au, Ni, Pd, Pt, and their alloys. It is found that the LREP model has successfully overcome the structural stability problem of traditional short-range potentials and resolved the energy and force jumps taking place in previous long-range potentials at cutoff radius without any truncated function. Importantly, the equations of state derived by the LREP model for the metals and alloys are in excellent agreement with those obtained from the Rose equation and experiments, indicating that the present model can relevantly predict the properties of metals and alloys at nonequilibrium state. Furthermore, the other calculated properties, such as the lattice constant, cohesive energy, elastic constants, and phonon spectra, also match well with those obtained by experiments or *ab initio* calculations.

DOI: 10.1103/PhysRevB.75.104101 PACS number(s): 34.20.Cf, 83.10.Rs, 61.43.Dq, 02.70.Ns

I. INTRODUCTION

Since the 1980s, a variety of empirical *n*-body potential models, such as the tight-binding approach based on the second moment approximation (TB-SMA),[1] the so-called embedded atom method (EAM),[2] and the Finnis-Sinclair (F-S) potential,[3] have been introduced and employed to study the bulk, surface, and cluster properties of metals. These potentials commonly truncate the energies and forces with a less than third nearest-neighbor short-range cutoff,[3–5] which could save computer time in large-scale simulations; nevertheless, they frequently encounter the unavoidable structural stability problem, i.e., they always predict the same energy for fcc and ideal hcp structures.[5,6] In order to overcome this problem, researchers try to construct new models for transition metals. For instance, considering the angular contributions, Baskes *et al.* proposed a modified EAM (MEAM) model for semiconductors and later extended it for transition metals.[7–9] This model does resolve the structural stability problem and improves some calculated properties of transition metals, such as surface energy; nevertheless, it also brings more application problems at the same time. For example, it is difficult to apply the MEAM model to disorder systems, such as liquid state and amorphous solid state, for the model parameters related to the angular factors are difficult to define in these circumstances. In fact, the atomic configuration of the first and second neighbor atoms is identical in fcc and ideal hcp structures. This is why the short-range potentials obtain the same calculated potential energy in both structures without considering the angular contributions. Consequently, a simple and effective way to differentiate the fcc and ideal hcp structures is adopting a longer cutoff radius, i.e., at least greater than the distance of the third nearest-neighbor atom, such as Cleri and Cai, respectively, have done in the TB-SMA potential and EAM potential.[10,11] Applying the long-range TB-SMA potential, Cleri calculated some physical properties of fcc and hcp metals and alloys, such as elastic constants and phonon spectra, but he did not calculate the structural stability of the metals.[10] On the other hand, using the long-range EAM potential, Cai reasonably calculated some properties of fcc metals and alloys and correctly predicted the structural stability; however, the predicted energy differences between fcc and ideal hcp structures are extremely underestimated when compared to the experimental values.[11] Besides, above long-range potentials also have an apparent shortage, i.e., the exponential forms in the repulsive term and *n*-body term are not equal to zero at the cutoff radius, resulting in that the calculated potential energies and forces have a little jump at this distance. A large number of these jumps will spoil the energy conservation or lead to unphysical behavior in dynamical simulations. To avoid this problem, a truncation function is necessary to be included, like Johnson, Adams, and Guellil have done.[5,12,13] If a potential can overcome this shortage without any truncation function, the computational process will be simplified and more computer time can be saved. Consequently, in order to resolve the problem and/or shortage mentioned in the above short-range and long-range potentials, we proposed a long-range empirical potential (LREP) model for transition metals under the framework of the second moment approximation of the tight-binding (TB-SMA) theory in the present study. In the following sections, we will first introduce the detailed formalism of the LREP model and then apply the model to calculate and/or predict some physical properties of fcc metals and alloys, such as lattice constants, cohesive energy, elastic constants, structural stability, equation of state, and phonon spectra.

II. THE LONG-RANGE EMPIRICAL POTENTIAL MODEL

According to the TB-SMA theory,[1] the total potential energy of an atom i is expressed as

$$E_i = E_i^R + E_i^B, \tag{1}$$

where E_i is the total potential energy of atom i, and E_i^R is the repulsive pair term expressed by

$$E_i^R = \frac{1}{2}\sum_{j\neq i} \phi(r_{ij}), \tag{2}$$

where r_{ij} is the distance between atoms i and j of the system at equilibrium state. $\phi(r_{ij})$ is expressed by a Born-Mayer type in the original TB-SMA scheme, i.e., $\phi(r_{ij}) = A\exp(-p(r_{ij}/r_0-1))$, while in the LREP model, it is expressed by a polynomial as follows:

$$\phi(r_{ij}) = \begin{cases} (r_{ij} - r_{c1})^m (x_0 + x_1 r_{ij} + x_2 r_{ij}^2 + x_3 r_{ij}^3 + x_4 r_{ij}^4), & r_{ij} \leqslant r_{c1}, \\ 0, & r_{ij} > r_{c1}, \end{cases} \tag{3}$$

where r_{c1} is a cutoff radius and x_0, x_1, x_2, x_3, and x_4 are the potential parameters to be fitted. The second term in Eq. (1) is the band-structure term, i.e., n-body term. Based on the second moment approximation to the tight-binding density of states, the energy of the d band is proportional to the square root of the second moment of the density of states and the band-structure term can be expressed in terms of a sum of the square of the hopping or transfer integrals, i.e.,

$$E_i^B = -\sqrt{\sum_j \varphi(r_{ij})}. \tag{4}$$

In the LREP model, $\varphi(r_{ij})$ is expressed by

$$\varphi(r_{ij}) = \begin{cases} \alpha(r - r_{c2})^n \exp\left[-\beta\left(\frac{r_{ij}}{r_0} - 1\right)\right], & r_{ij} \leqslant r_{c2}, \\ 0, & r_{ij} > r_{c2}, \end{cases} \tag{5}$$

where r_{c2} is also a cutoff radius. α and β are two adjustable parameters, i.e., potential parameters. Note that r_0, in the present study, is also treated as an adjustable parameter. If necessary, r_{c1} and r_{c2} also can be treated as free parameters in the fitting procedure. m and n, in Eqs. (3) and (5), are generally adopted integer values and can be adjustable according to the specific element. From the forms expressed in Eqs. (3) and (5), one sees clearly that if $m > 3$ and $n > 3$, the terms of $(r_{ij} - r_{c1})^m$ and $(r - r_{c2})^n$ can ensure $\phi(r_{ij})$, $\varphi(r_{ij})$ and their first derivatives smoothly go to zero at cutoff radii. In other words, the total energy and force in the present potential can keep continuous and smooth in the whole calculated range and thus, completely remove the cutoff problem taking place in the previously mentioned long-range potentials.

III. APPLICATION TO fcc METALS

A. Construction of the pure fcc potentials

For the pure fcc transition metals, the potential parameters are determined by fitting their basic physical properties obtained from experiments, i.e., cohesive energy, lattice constants, elastic constants. Besides, when a metal is in equilibrium state, its first derivative dE of potential energy and the stress σ of each unit cell should be equal to zero, so $dE(a)|_{a=a_0}=0$ and $\sigma(a)|_{a=a_0}=0$ have been regarded as two fitting conditions in the present study so as to confirm the equilibrium state of a structure. Different from the short-range potential, we adopted longer cutoff radii for all the fcc metals, i.e., $r_{c1} > r_4$ and $r_{c2} > r_7$, where r_4 and r_7 are the fourth and seventh neighbor distances, respectively. Table I displays all the fitted potential parameters for six fcc metals, i.e., Cu, Ag, Au, Ni, Pd, and Pt. Table II gives the fitted and experimental properties of the six metals, from which one can see clearly that the fitted properties completely match with their experimental values. In addition, the first derivatives of energy dE (eV/Å) and the remnant stresses σ (Mbar) are all less than 1×10^{-6}, indicating that the fitted structures of these metals are very close to the equilibrium states.

Figure 1 shows the repulsive terms E^R and n-body terms E^B of total potential energies calculated from the newly constructed potentials for Cu, Ag, Au, Ni, Pd, and Pt. From the figure, one sees that both the repulsive terms and n-body terms keep smooth in the whole calculated range and smoothly go to zero at cutoff radii, indicating that the forms of Eqs. (3) and (5) can really ensure the repulsive term and n-body terms smoothly go to zero at the cutoff distance.

TABLE I. The fitted potential parameters for Cu, Ag, Au, Ni, Pd, and Pt.

	Cu	Ag	Au	Ni	Pd	Pt
m	4	4	4	4	4	4
n	6	6	6	6	6	6
r_{c1} (Å)	6.100	6.375	6.400	6.000	6.300	6.440
r_{c2} (Å)	7.800	7.950	8.500	7.500	7.800	8.500
x_0 (eV Å^{-m})	0.123554	0.235139	0.346813	0.173210	0.311702	0.362085
x_1 (eV Å^{-m-1})	−0.134361	−0.247471	−0.350701	−0.198386	−0.333143	−0.378121
x_2 (eV Å^{-m-2})	0.0543818	0.0983304	0.133662	0.0840575	0.134071	0.149113
x_3 (10^{-2} eV Å^{-m-3})	−0.981194	−1.748544	−2.273741	−1.596247	−2.413259	−2.610984
x_4 (10^{-3} eV Å^{-m-4})	0.675816	1.174278	1.456262	1.172505	1.642024	1.706176
α (10^{-4} eV^2 Å^{-n})	0.656618	0.805877	1.011750	0.811753	1.560181	2.678379
β	1.836569	2.951121	5.580155	0.376885	4.472177	4.354578
r_0 (Å)	2.552655	2.892067	2.884996	2.489016	2.750645	2.771859

TABLE II. Fitted results of lattice constants (a), cohesive energy (E_c), and elastic constants (C_{11}, C_{12}, and C_{44}) by the LREP model together with their experimental values for Cu, Ag, Au, Ni, Pd, and Pt.

	Methods	Cu	Ag	Au	Ni	Pd	Pt
a (10^{-10} m)	LREP	3.61	4.09	4.08	3.52	3.89	3.92
	Expt.[a]	3.61	4.09	4.08	3.52	3.89	3.92
E_c (eV)	LREP	3.49	2.95	3.81	4.44	3.89	5.84
	Expt.[a]	3.49	2.95	3.81	4.44	3.89	5.84
C_{11} (Mbar)	LREP	1.762	1.315	2.016	2.481	2.341	3.47
	Expt.[a,b]	1.762	1.315	2.016	2.481	2.341	3.47
C_{12} (Mbar)	LREP	1.249	0.973	1.697	1.549	1.761	2.51
	Expt.[a,b]	1.249	0.973	1.697	1.549	1.761	2.51
C_{44} (Mbar)	LREP	0.818	0.511	0.454	1.242	0.712	0.765
	Expt.[a,b]	0.818	0.511	0.454	1.242	0.712	0.765

[a]Reference 14.
[b]Reference 15.

B. Structural stability

In the fitting procedure, we do not consider whether the fcc crystal structure is more stable than a bcc or hcp one. However, it is known that the global stability is very important to test the reliability of a potential. Based on the newly constructed LREP potentials, we calculate the energies of metastable structures, i.e., bcc and ideal hcp structures of the six fcc metals. The bcc and hcp structures are first optimized using the constructed potentials and then the potential energies of the metastable structures are calculated. It is noted that the atomic volume is allowed to vary during the present optimization, differing from other constant-atomic-volume methods, in which the atomic volume is assumed to be constant in various structures.[11,16]

Table III shows the calculated energy differences between the metastable structures and the fcc one, i.e., $\Delta E_{\mathrm{fcc}\rightarrow\mathrm{bcc}}$, $\Delta E_{\mathrm{fcc}\rightarrow\mathrm{hcp}}$, $\Delta E_{\mathrm{fcc}\rightarrow\mathrm{sc}}$, and $\Delta E_{\mathrm{fcc}\rightarrow\mathrm{dia}}$, where sc and dia denote the simple cubic structure and diamond structure, respectively. For comparison, the results obtained from Cai's EAM potential, experimental observations, and *ab initio* calculations are also listed in Table III. In the present study, *ab initio* calculations are conducted by using the Cambridge serial total energy package (CASTEP).[17] In *ab initio* calculation, the nonlocal ultrasoft pseudopotentials have been used, together with a kinetic energy cutoff of 350 eV and the PW91 generalized-gradient approximation (GGA) exchange-correlation functional.[18] The integration in the Brillouin zone is done in a mesh of $11\times11\times11$ special k points determined according to the so-called Monkhorst-Pack scheme. If there is not any special note, the *ab initio* calculations in the following sections also adopt the same setting. From Table III, one sees that the values of energy differences predicted by the present model quantitatively match with those obtained from experiments or *ab initio* calculations. Both the calculated results and experimental ones indicate that fcc structure has the lowest potential energy among fcc, bcc, hcp, simple cubic, and diamond structures, reflecting well the fact that the equilibrium states of these metals are in fcc structures. However, inspecting the values of $\Delta E_{\mathrm{bcc}\rightarrow\mathrm{fcc}}$ and $\Delta E_{\mathrm{hcp}\rightarrow\mathrm{fcc}}$ predicted by Cai's EAM model, one sees that they have been systematically underestimated compared to the experimental results, especially for $\Delta E_{\mathrm{hcp}\rightarrow\mathrm{fcc}}$, the maximum relative error is beyond 94%. Apparently, the present model is more relevant than that proposed by Cai in predicting the structural stability of fcc transition metals.

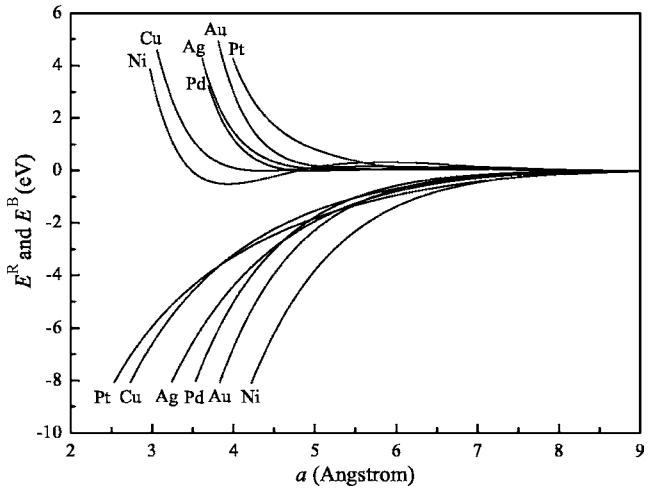

FIG. 1. The repulsive terms E^R and n-body terms E^B of potential energies for Cu, Ag, Au, Ni, Pd, and Pt, respectively.

In the above paragraph, we have satisfactorily predicted the energy differences between the fcc structures and their metastable ones based on the constructed LREP potentials. For an excellent potential model, it should not only satisfactorily predict the structural stability of the metals but also correctly calculate other properties of their metastable structures. Consequently, based on the constructed LREP potentials, we calculated the lattice constants, elastic modulus, and elastic constants for the metastable bcc and hcp structures of Cu, Ag, Au, Ni, Pd, and Pt, and the results are listed in Table

TABLE III. The structural energy differences ΔE (eV) obtained from EAM potential, the LREP model, *ab initio* calculations, and experimental observations, respectively. sc and dia denote the simple cubic structure and diamond structure, respectively. For hcp structures, $c/a=1.632\,99$.

	Methods	Cu	Ag	Au	Ni	Pd	Pt
$\Delta E_{fcc\rightarrow bcc}$	EAM[a]	0.0220	0.0254	0.0265	0.0330	0.0370	0.0430
	LREP	0.0318	0.0470	0.0498	0.0608	0.0801	0.1080
	Expt.[b]	0.0400	0.0300	0.0400	0.0700	0.1000	0.1500
$\Delta E_{fcc\rightarrow hcp}$	EAM[a]	0.0012	0.0012	0.0005	0.0010	0.0016	0.0011
	LREP	0.0081	0.0031	0.0070	0.0196	0.0185	0.0217
	Expt.[b]	0.0060	0.0030	0.0050	0.0150	0.0200	0.0200
$\Delta E_{fcc\rightarrow sc}$	LREP	0.4940	0.3712	0.3398	0.6958	0.4529	0.4763
	Ab initio	0.4648	0.3573	0.2197	0.6356	0.5199	0.5108
$\Delta E_{fcc\rightarrow dia}$	LREP	1.2401	0.8839	0.6918	1.9572	1.0488	0.7049
	Ab initio	1.0402	0.8384	0.7541	1.2002	1.2214	1.1760

[a]Reference 11.
[b]Reference 8.

IV. For comparison, the results derived from *ab initio* calculations are also listed in the table. First, inspecting the lattice constants in Table IV, one sees that the results derived from the LREP model for all the bcc structures and for the hcp structures of Cu, Ag, Ni, and Pd are in good agreement with those derived from *ab initio* calculations, with the largest relative error being around 2.02%. For the hcp structures of Au and Pt, the agreement between the results calculated from both methods are also good, with the largest relative error being 4.35%. Moreover, inspecting the elastic modulus and elastic constants derived from the LREP model, one sees that although they have some departures compared to those de-

TABLE IV. The lattice constants, cohesive energies, bulk modulus, and elastic constants for the metastable bcc and hcp structures of Cu, Ag, Au, Ni, Pd, and Pt, respectively. The properties in the upper rows are from the LREP model and those in the lower rows are from *ab initio* calculations using CASTEP program. a and c are expressed in 10^{-10} m and B, C_{11}, C_{12}, C_{13}, C_{33}, and C_{44} are expressed in Mbar.

	Cu		Ag		Au		Ni		Pd		Pt	
	bcc	hcp	bcc	hcp	bcc	hcp	bcc	hcp	bcc	hcp	bcc	hcp
a	2.865	2.553	3.271	2.887	3.250	2.874	2.795	2.485	3.102	2.742	3.110	2.765
	2.866	2.538	3.274	2.892	3.317	2.925	2.811	2.491	3.114	2.745	3.163	2.765
c		4.176		4.781		4.771		4.075		4.555		4.551
		4.204		4.807		4.890		4.128		4.607		4.758
B	1.282	1.346	0.979	1.100	1.650	1.845	1.505	1.687	1.648	1.921	2.516	2.759
	1.366	1.499	1.387	0.999	1.378	1.438	2.010	1.916	1.801	1.778	2.474	2.555
C_{11}	1.284	2.261	0.811	1.653	1.477	2.386	1.527	3.149	1.361	2.791	2.251	3.808
	0.828	2.624	0.600	1.757	1.169	2.276	1.444	2.973	1.688	2.522	1.811	4.274
C_{12}	1.281	1.040	1.063	0.863	1.736	1.642	2.251	1.256	1.792	1.642	2.648	2.447
	1.635	1.045	1.186	0.781	1.482	1.200	1.535	1.398	1.858	1.706	2.805	1.979
C_{13}		0.787		0.747		1.514		0.823		1.414		2.211
		0.837		0.542		0.985		1.312		1.240		1.728
C_{33}		2.301		1.876		2.493		3.077		2.762		3.477
		2.806		1.775		2.120		3.266		2.650		3.748
C_{44}	0.850	0.357	0.616	0.278	0.527	0.244	1.188	0.513	0.772	0.345	0.908	0.442
	0.892	0.308	0.541	0.269	0.557	0.250	1.229	0.486	0.908	0.298	1.589	0.159

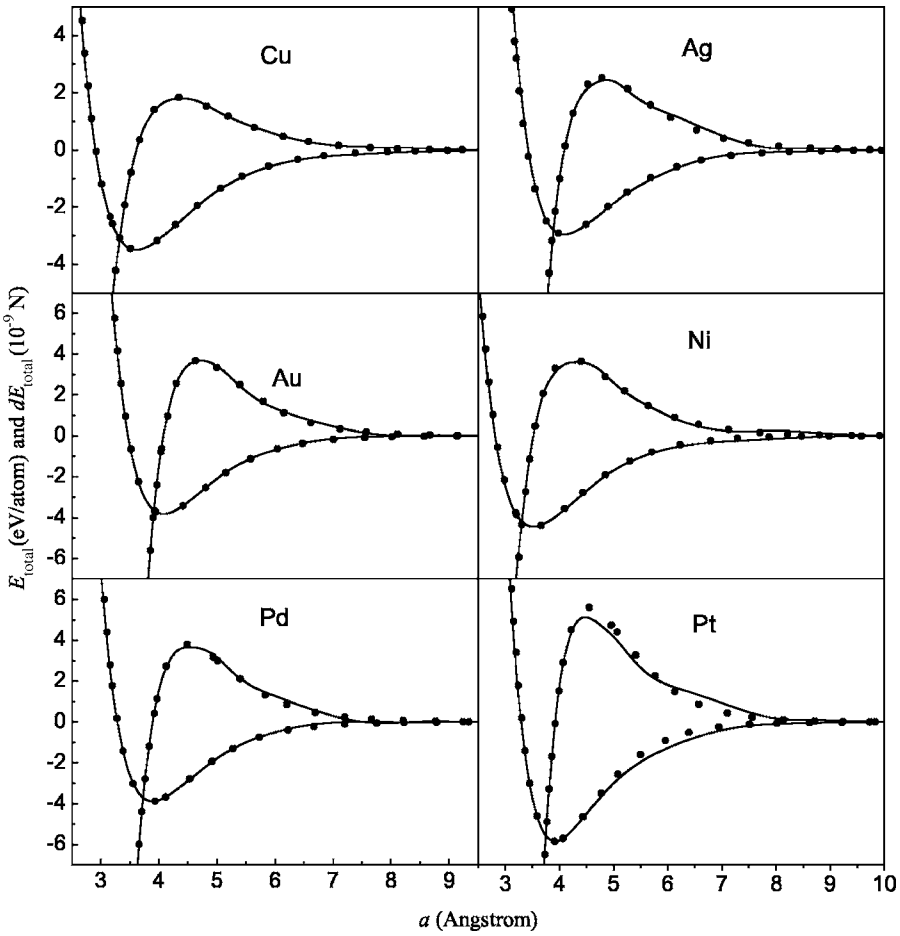

FIG. 2. Total energies E_{total} and their derivatives dE_{total} as a function of lattice constant a calculated from the LREP model (solid lines) and Rose equation (scattered points), respectively, for Cu, Ag, Au, Ni, Pd, and Pt.

duced from *ab initio* calculations, most of the relative errors are less than 30%, exhibiting a reasonable agreement with the results obtained by *ab initio* calculations. In short, taking account of the computation error of the *ab initio* scheme in elastic calculations, one can conclude that the present predictions from the LREP model are matched well with those from *ab initio* calculations, suggesting the present model is also relevant in predicting the lattice constants and elastic properties of the simple metastable structures of fcc transition metals.

C. Equation of state

In atomistic modeling of metals and alloys, a distance is always different from the equilibrium one, and therefore another important approach to evaluate the relevance of a constructed potential is to check whether the potential can describe the atomic interaction of a system at nonequilibrium states, i.e., to derive the equation of state (EOS) from the potential and then compare it with that obtained from theory or experiments.

Theoretically, the frequently used EOS is the Rose equation,[19] which has been considered a universal EOS for the solids. Therefore, based on the constructed LREP potentials, we calculated the EOSs, i.e., the total potential energy as a function of the lattice constant, for Cu, Ag, Au, Ni, Pd, and Pt, and then compared them with those derived from the Rose equation. Figure 2 shows the EOSs derived from the LREP model and the Rose equation, respectively. One sees from the figure that the results derived from the LREP model are in good agreement with those derived from the Rose equation even far from the equilibrium state. The agreement is best for Cu, Ag, Au, Ni, and Pd, and good for Pt. From the figure, one also sees that the total energy derived from the LREP model can keep smooth in the whole calculated range and smoothly go to zero at cutoff radius, indicating that this model does overcome the energy jumps at cutoff radius which take place in Cleri's TB-SMA potential and Cai's EAM potential. During MD simulation, the interatomic force deduced from the derivative of total energy is a very important physical variable, which directly affects the simulation result. In general, for a curve of force versus distance, continuousness, no sharp fluctuations, and no odd points are all the basic features to ensure obtaining the correct simulation result. In Fig. 2, the derivatives of total energy calculated from the LREP model for Cu, Ag, Au, Ni, Pd, and Pt metals together with those deduced from the Rose equation are shown. From the figure, one sees that for all the studied metals, the derivatives of total energy derived from the LREP model can keep smooth in the whole calculated range and smoothly go to zero at cutoff radius, and the calculated results are in good agreement with those derived from the Rose equation, implying the LREP model can relevantly describe the atomic interactions in the fcc metals and avoid the unphysical behaviors that may emerge in simulations.

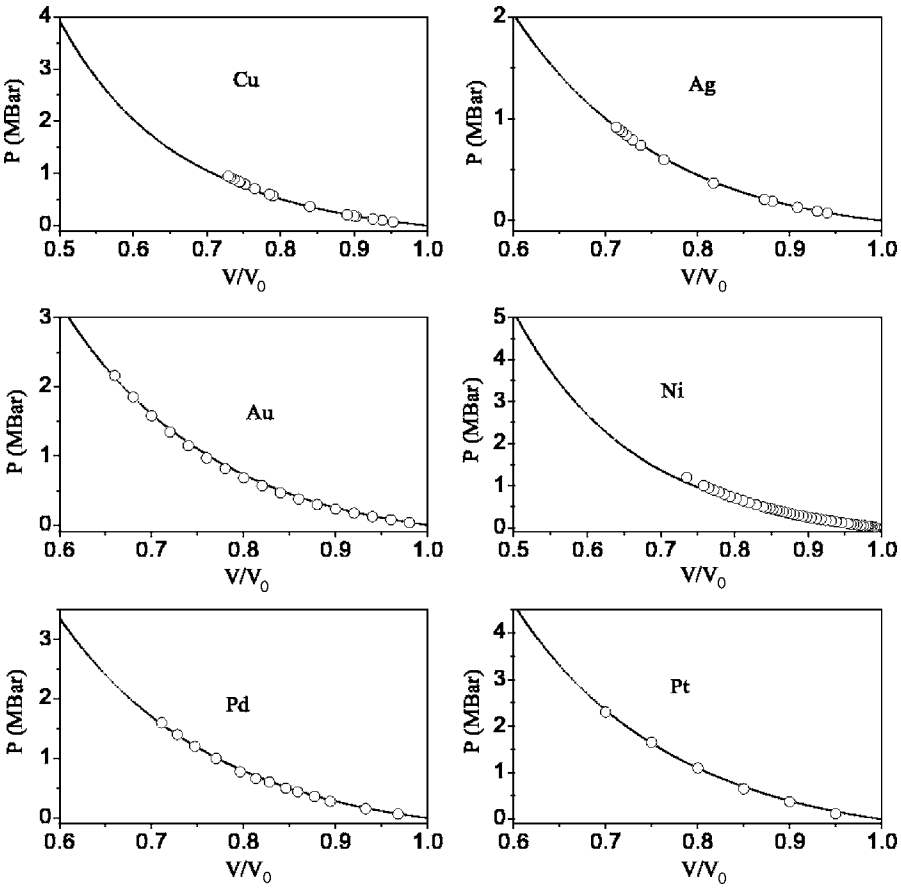

FIG. 3. The relationships of pressure vs relative volume obtained from the LREP model (solid lines) and experiments (scattered points), respectively, for Cu, Ag, Au, Ni, Pd, and Pt. The experimental values are from Refs. 20–23.

Experimentally, the EOS is generally expressed by pressure as a function of relative volume, i.e., *P-V* relationship. We also calculated the *P-V* relationships for the six fcc metals based on the LREP model and compared them with their respective experimental values in Fig. 3. It is clear that the agreement between the calculated results and experimental values is excellent, further confirming that the LREP model can reasonably describe atomic interactions at nonequilibrium state in the fcc metals.

D. Phonon spectra

The ability to predict the phonon dispersion curves is also considered to be useful evidence for validating the reliability of an empirical potential model. To obtain the phonon spectra, there are basically three approaches in determining the force constants, i.e., analytic calculation, super-cell calculation, and linear-response calculation.[24] In the present study, we perform analytic calculation with the LREP model to obtain the phonon spectra for the fcc structures of Cu, Ag, Au, Ni, Pd, and Pt. Based on the Born–von Kármán model,[25] using the constructed LREP potentials, the interatomic force constants $\Phi_{\alpha\beta}(\vec{r}_{ij})$ between the atom i and atom j can be obtained under the harmonic approximation. Consequently, the phonon spectra can be calculated through the dynamical matrix $D_{\alpha\beta}(\vec{q},kk')$, which is the Fourier transformation of the interatomic force constant,

$$|D_{\alpha\beta}(\vec{q},kk') - m_k m_{k'}\omega^2(\vec{q})\delta_{\alpha\beta}\delta_{kk'}| = 0,$$

where m_k is the mass of the k atom, ω is the phonon frequency, $\vec{q}$ is the wave vector, and δ is the Kronecker function.

Based on the constructed LREP potentials, the phonon spectra of the six fcc metals are obtained and shown in Fig. 4. For comparison, the experimental results are also plotted in the figure. In fact, in the long wavelength limit, the phonon dispersion curves are directly related to the elastic constants which have been fitted when constructing the potentials, so one can see from Fig. 4 that the results calculated from the LREP model are quite consistent with those obtained by experimental observations in the long wavelength limit. In the short wavelength limit, one sees that the shapes of calculated results are also very similar to those obtained by experiments, although there are some departures between calculated values and experimental ones. As a whole, the agreement is good for Cu, Ag, and Pd, and fair for Au, Ni, and Pt, indicating that the LREP model can reasonably reveal the lattice dynamics behavior in fcc metals.

IV. APPLICATION TO fcc-fcc METALLIC ALLOYS

In preceding sections, the present model has been used to investigate pure metal systems, and the results are satisfactory. In the present section, we will show that the proposed LREP model can also be applied to fcc-fcc alloy systems.

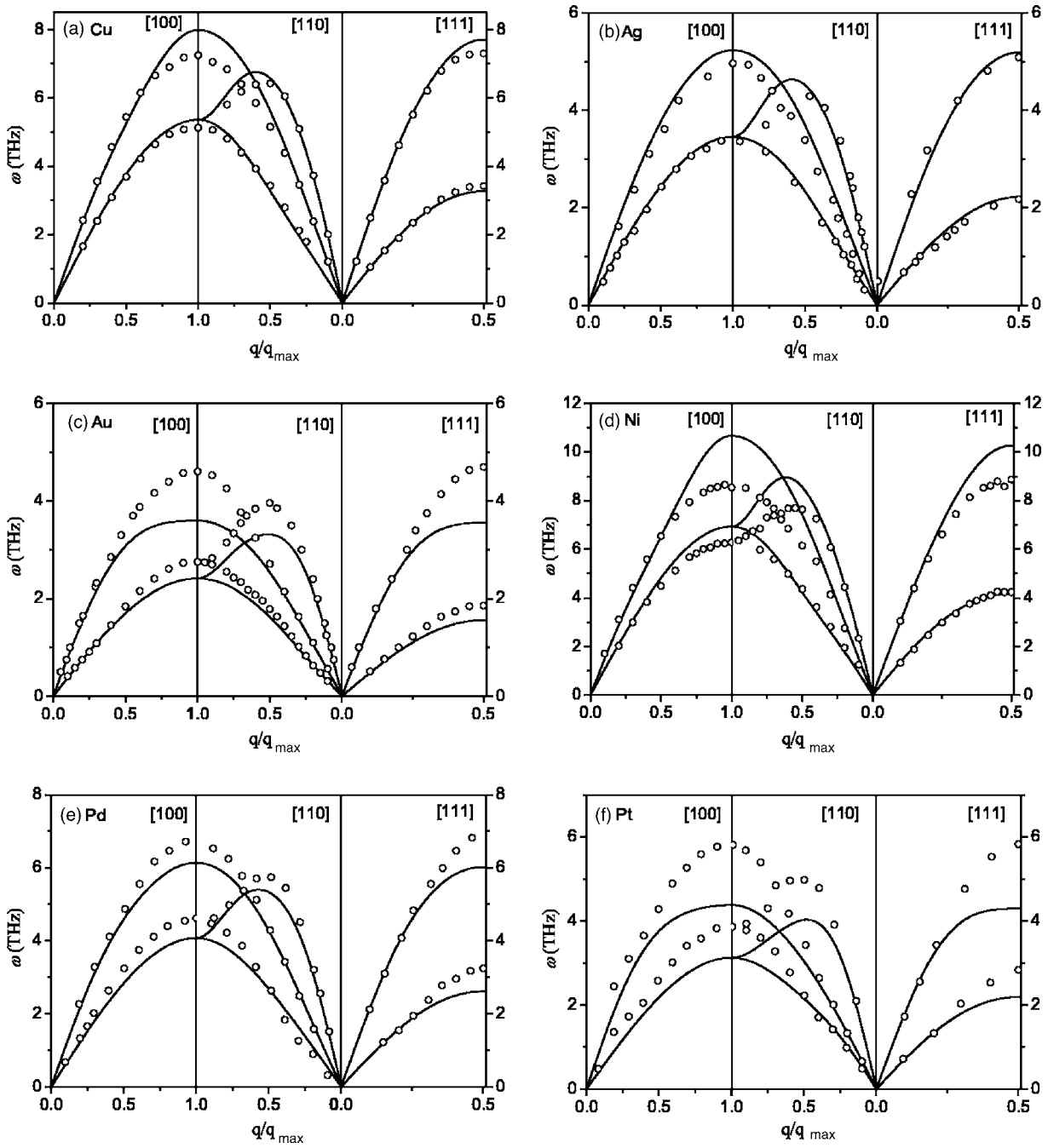

FIG. 4. The phonon spectra obtained from the LREP model (solid lines) and experiments (scattered points) for Cu, Ag, Au, Ni, Pd, and Pt at zero pressure. The experimental values are from Refs. 26–31.

Here we selected the Ag-Cu, Cu-Au, and Ag-Au binary metal systems as the examples and present the results obtained from the metallic alloys in the three alloy systems.

A. Construction of the fcc-fcc cross potentials

It is a challenging task to determine the alloy potential parameters by directly fitting the properties of the alloys, as there are not sufficient available experimental data related to the alloy compounds. To avoid the difficulty, the assumption is commonly made that the alloy potential is a function of the monatomic potentials. For example, in 1985, Foiles proposed an alloy model under the EAM frameworks in which the embedding function and electron density function are directly taken from monatomic models and the pair potential is assumed to be the geometric mean of monatomic ones.[32] Later, Johnson also proposed a similar alloy model in which the pair potential is assumed to be a density-weighted combination of monatomic ones.[33] Although these alloy models make it easy to obtain a cross potential for alloys, they are only the approximate ones based on some assumptions. It is well known that the *ab initio* calculation based on quantum mechanics is a reliable way to acquire some physical prop-

TABLE V. The fitted potential parameters for Ag-Cu, Cu-Au, and Au-Ag alloys.

	Ag-Cu	Cu-Au	Au-Ag
m	4	4	4
n	6	6	6
r_{c1} (Å)	6.000000	6.000000	5.706344
r_{c2} (Å)	7.500000	7.800000	6.841334
x_0 (eV Å^{-m})	0.233892	0.292061	0.468608
x_1 (eV Å^{-m-1})	−0.249618	−0.311393	−0.460405
x_2 (eV Å^{-m-2})	0.101643	0.127695	0.175479
x_3 (10^{-2} eV Å^{-m-3})	−1.859480	−2.336064	−2.993292
x_4 (10^{-3} eV Å^{-m-4})	1.284024	1.602712	1.885116
α (10^{-3} eV^2 Å^{-n})	0.204474	0.379239	1.485145
β	2.963432	2.915843	3.122075
r_0 (Å)	2.646736	2.671407	2.816507

erties of some possible intermetallic compounds.[34–36] Consequently, *ab initio* calculations are carried out in the present study, and the lattice constants, cohesive energies, and elastic modulus of some hypothetic alloys, i.e., $L1_2$ A_3B alloys, $B2$ AB alloys, and $L1_2$ AB_3 alloys (where A and B are any two elements among Cu, Ag, and Au), are obtained and then applied in fitting the Ag-Cu, Cu-Au, and Ag-Au cross potentials. The parameters of the fitted Ag-Cu, Cu-Au, and Ag-Au cross potentials are listed in Table V. After constructing the cross potentials, we will apply them to calculate some properties of alloys in the following sections so as to validate their reliabilities in describing the atomic interactions in fcc-fcc alloys.

B. Equation of state

As mentioned previously, calculating the EOS can evaluate whether a potential can correctly predict the properties of metals or alloys at the nonequilibrium state. Therefore, we calculated the total energies as a function of lattice constant for some Ag-Cu, Cu-Au, and Ag-Au alloys based on the constructed LREP potentials, and the results are shown in Fig. 5. For comparison, the corresponding results derived from the Rose equation are also shown in the figure. From the figure, one sees clearly that the total energies calculated from the LREP model are quite agreeable with those derived from the Rose equation in the whole calculated range, indicating that the present model can satisfactorily describe the energy state of an fcc-fcc alloy even far from the equilibrium state. Moreover, the derivatives of total energies calculated from the present model and the Rose equation, respectively, for these alloys are also shown in Fig. 5. One sees from the figure that the agreement between the derivatives derived from the LREP model and those derived from the Rose equation is excellent, indicating the present model can reasonably reflect the atomic interactions in fcc-fcc alloys. Further inspecting the curves in Fig. 5, one sees that the total energies and their derivatives can keep smooth in the whole calculated range and both of them can smoothly go to zero at cutoff radius, indicating that the present model can also over-

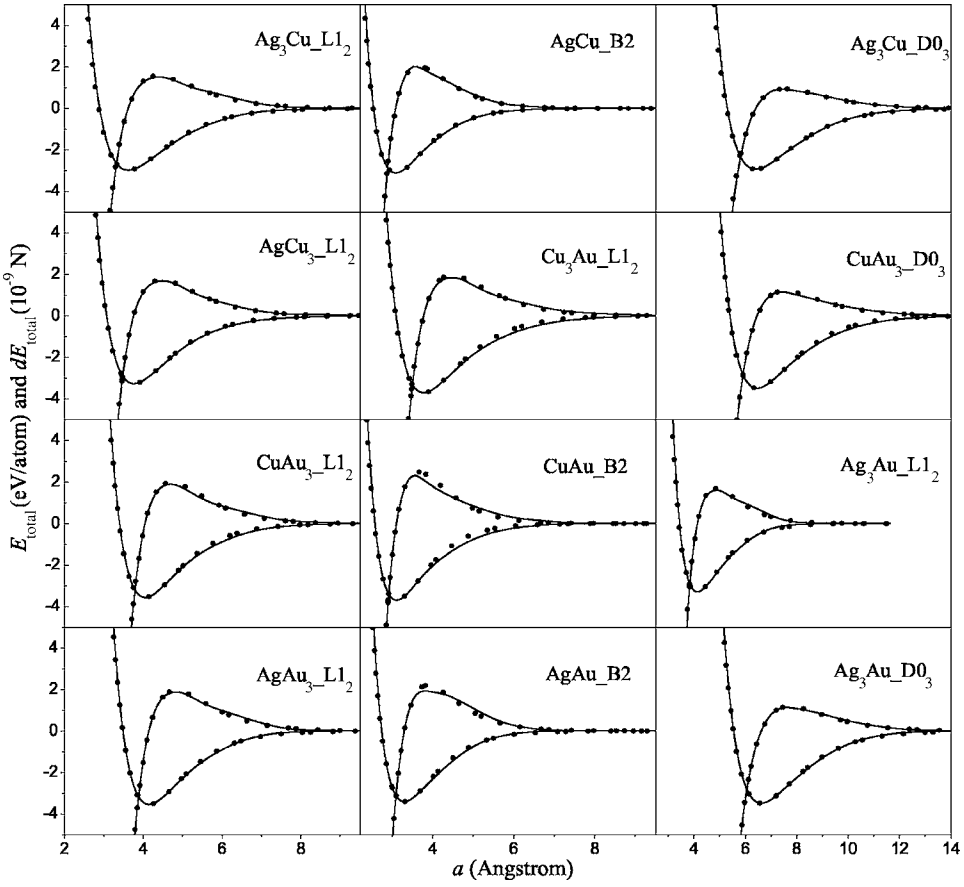

FIG. 5. The total energies E_{total} and their derivatives dE_{total} calculated from the LREP model (solid lines) and Rose equation (scattered points), respectively, for Ag-Cu, Cu-Au, and Ag-Au alloys with different structures.

TABLE VI. The lattice constants a (Å), cohesive energies E_c (eV), elastic constants C_{ij} (Mbar), and bulk modulus B (Mbar) derived from the LREP model and *ab initio* calculations, respectively.

Compounds	Methods	a	E_c	C_{11}	C_{12}	C_{44}	B
Ag_3Cu-$L1_2$	LREP	4.0073	2.9764	1.2562	1.0058	0.4482	1.0892
	Ab initio	4.0089	3.0091	1.2744	0.9918	0.6026	1.0860
$AgCu_3$-$L1_2$	LREP	3.7556	3.2729	1.4722	1.1822	0.5931	1.2789
	Ab initio	3.7551	3.2643	1.5001	1.1699	0.6762	1.2800
AgCu-$B2$	LREP	3.0829	3.1106	1.2072	1.1142	0.4783	1.1452
	Ab initio	3.0829	3.0951	0.9652	1.2398	0.3145	1.1483
Ag_3Cu-$D0_3$	LREP	6.3990	2.9246	0.8558	1.0808	0.5358	1.0058
	Ab initio	6.3784	2.9694	0.9726	1.0920	0.3991	1.0522
$AgCu_3$-$D0_3$	LREP	5.9870	3.2211	1.0724	1.2306	0.6366	1.1779
	Ab initio	5.9694	3.2236	1.0613	1.3522	0.6017	1.2552
Cu_3Au-$L1_2$	LREP	3.7722	3.7058	1.7177	1.3191	0.5289	1.4519
	Ab initio	3.7706	3.5934	1.8133	1.2847	0.6045	1.4609
$CuAu_3$-$L1_2$	LREP	4.0455	3.5616	1.5575	1.3899	0.3175	1.4458
	Ab initio	4.0542	3.7287	1.6301	1.3406	0.4246	1.4371
CuAu-$B2$	LREP	3.1029	3.6930	1.7465	1.2552	0.2969	1.4189
	Ab initio	3.1029	3.6800	1.3355	1.4713	0.4391	1.4261
Cu_3Au-$D0_3$	LREP	6.0080	3.6234	1.1396	1.4219	0.5829	1.3278
	Ab initio	6.0024	3.5469	1.3908	1.4993	0.6984	1.4631
$CuAu_3$-$D0_3$	LREP	6.4490	3.4922	1.1865	1.4283	0.3783	1.3477
	Ab initio	6.4544	3.6857	1.0914	1.5114	0.3265	1.3714
Ag_3Au-$L1_2$	LREP	4.1253	3.2842	1.2677	1.0346	0.2155	1.1123
	Ab initio	4.1227	3.2174	1.2974	1.0289	0.5254	1.1184
$AgAu_3$-$L1_2$	LREP	4.1447	3.5406	1.4441	1.3251	0.1939	1.3648
	Ab initio	4.1488	3.6415	1.6101	1.2301	0.4719	1.3567
AgAu-$B2$	LREP	3.2955	3.4075	1.1516	1.1304	0.1006	1.1375
	Ab initio	3.2955	3.4004	0.9098	1.2511	0.2392	1.1373
Ag_3Au-$D0_3$	LREP	6.5990	3.2100	0.8366	1.1191	0.2860	1.0250
	Ab initio	6.5676	3.1774	1.0482	1.0779	0.5084	1.0681
$AgAu_3$-$D0_3$	LREP	6.6160	3.4777	1.1233	1.3382	0.2324	1.2666
	Ab initio	6.6075	3.6014	1.0098	1.3971	0.5241	1.2679

come the energy and force jumps at cutoff distance in alloy systems.

C. Elastic properties

During the fitting procedure, we only fitted the lattice constants, cohesive energies, and elastic modulus of $L1_2$ A_3B alloys, $B2$ AB alloys, and $L1_2$ AB_3 alloys. For further evaluating the constructed cross potentials, the lattice constants, cohesive energies, elastic modulus, and elastic constants of more hypothetical alloys in Ag-Cu, Cu-Au, and Ag-Au systems are calculated and the results are listed in Table VI. For comparison, the results deduced directly from *ab initio* calculations are also listed in the table. First, one can see from the table that the reproduced lattice constants are in good agreement with those derived from *ab initio* calculations, as the largest error between the results derived from both methods is only 0.32%. Besides, the errors between the reproduced cohesive energies and those derived from *ab initio* calculations are all less than 6%, suggesting the agreement between both methods is also good. As for the elastic constants, one can see that the agreement of C_{12} is the best with the largest relative error being 14.68%, that of C_{11} is the secondary with the largest relative error being 30.77%, and

that of C_{44} is the worst with the largest relative error being 58.98%. Finally, inspecting the elastic modulus, one can see that the agreement between both methods is also good, for the relative errors are all less than 10%. Considering the computational error of the *ab initio* scheme in elastic calculations, one can conclude that all the reproduced results are in good agreement with those derived from *ab initio* calculations, suggesting that the LREP model is relevant to reproduce the lattice constants and cohesive energy of fcc-fcc alloys, and can reasonably reflect the elastic behaviors in the alloys.

V. CONCLUDING REMARKS

A long-range empirical potential has been developed and satisfactorily applied to six fcc metals and their alloys. The LREP model has successfully overcome the structural stability problem in traditional short-range potentials and in some long-range potentials, and resolved the energy and force jumps in Cai's EAM potential and Cleri's TB-SMA potential. The other reproduced properties, such as the lattice constant, cohesive energy, elastic constants, and phonon spectra, are also quite agreeable with the experimental values or the results derived from *ab initio* calculations. Especially, the EOSs reproduced by the LREP model are in good agreement with those obtained from the Rose equation and experiments, indicating that the present model can not only describe the properties at equilibrium state but also predict those at nonequilibrium state. The present model has a simple analytic form and can be widely applied in general calculations or large-scale simulations of the metals and alloys (including their order and disorder states).

ACKNOWLEDGMENTS

The authors are grateful to the financial support from the National Natural Science Foundation of China (Grant No. 50531040), the Ministry of Science and Technology of China (Grant No. 2006CB605201), and the Administration of Tsinghua University.

*Corresponding author. Electronic address: lijiahao02@mails.tsinghua.edu.cn

[1] D. Tomanek, A. A. Aligia, and C. A. Balseiro, Phys. Rev. B **32**, 5051 (1985).
[2] M. S. Daw and M. I. Baskes, Phys. Rev. Lett. **50**, 1285 (1983).
[3] M. W. Finnis and J. E. Sinclair, Philos. Mag. A **50**, 45 (1984).
[4] R. A. Johnson, Phys. Rev. B **37**, 3924 (1988).
[5] R. A. Johnson and D. J. Oh, J. Mater. Res. **4**, 1195 (1989).
[6] X. D. Dai, Y. Kong, and J. H. Li, J. Phys.: Condens. Matter **18**, 4527 (2006).
[7] M. I. Baskes, J. S. Nelson, and A. F. Wright, Phys. Rev. B **40**, 6085 (1989).
[8] M. I. Baskes, Phys. Rev. B **46**, 2727 (1992).
[9] M. I. Baskes and R. A. Johnson, Modell. Simul. Mater. Sci. Eng. **2**, 147 (1994).
[10] Fabrizio Cleri and Vittorio Rosato, Phys. Rev. B **48**, 22 (1993).
[11] J. Cai and Y. Y. Ye, Phys. Rev. B **54**, 8398 (1996).
[12] J. B. Adams and S. M. Foiles, Phys. Rev. B **41**, 3316 (1990).
[13] A. M. Guellil and J. B. Adams, J. Mater. Res. **7**, 639 (1992).
[14] C. Kittel, *Introduction to Solid State Physics* (Wiley, New York, 1996).
[15] D. R. Lide, *CRC Handbook of Chemisty and Physics* (CRC, New York, 2003).
[16] D. J. Oh and R. A. Johnson, J. Mater. Res. **3**, 471 (1988).
[17] M. D. Segall, P. L. Lindan, M. J. Probert, C. J. Pickard, P. J. Hasnip, S. J. Clark, and M. C. Payne, J. Phys.: Condens. Matter **14**, 2717 (2002).
[18] J. P. Perdew and Y. Wang, Phys. Rev. B **45**, 13244 (1992).
[19] J. H. Rose, J. R. Smith, F. Guinea, and J. Ferrante, Phys. Rev. B **29**, 2963 (1984).
[20] H. K. Mao, P. M. Bell, J. W. Shaner, and D. J. Steinberg, J. Appl. Phys. **49**, 3276 (1978).
[21] O. L. Anderson, D. G. Isaak, and S. Yamamoto, J. Appl. Phys. **65**, 1534 (1989).
[22] N. C. Holmes, J. A. Moriarty, G. R. Gathers, and W. J. Nellis, J. Appl. Phys. **66**, 2962 (1989).
[23] R. Kinslow, *High-Velocity Impact Phenomena* (Academic, New York, London, 1970).
[24] G. M. Day, S. L. Price, and M. Leslie, J. Phys. Chem. B **107**, 10919 (2003).
[25] P. Brüesch, *Phonons: Theory and Experiments I* (Springer-Verlag, Berlin, 1982).
[26] R. M. Nicklow, G. Gilat, H. G. Smith, L. J. Raubenheimer, and M. K. Wilkins, Phys. Rev. **164**, 922 (1967).
[27] W. A. Kamitakahara and B. N. Brockhouse, Phys. Lett. **29A**, 639 (1969).
[28] L. W. Lynn, H. G. Smith, and R. M. Nicklow, Phys. Rev. B **8**, 3493 (1973).
[29] R. J. Birgeneau, J. Cords, G. Dolling, and A. D. Woods, Phys. Rev. **136**, A1359 (1964).
[30] A. P. Miller and B. N. Brockhouse, Can. J. Phys. **49**, 704 (1971).
[31] D. H. Dutton, B. N. Brockhouse, and A. P. Miller, Can. J. Phys. **50**, 2915 (1972).
[32] S. M. Foiles, Phys. Rev. B **32**, 7685 (1985).
[33] R. A. Johnson, Phys. Rev. B **39**, 12554 (1989).
[34] D. E. Luzzi, M. Yan, M. Šob, and V. Vitek, Phys. Rev. Lett. **67**, 1894 (1991).
[35] M. Yan, M. Šob, D. E. Luzzi, V. Vitek, G. J. Ackland, M. Methfessel, and C. O. Rodriguez, Phys. Rev. B **47**, 5571 (1993).
[36] R. Siegl, M. Yan, and V. Vitek, Modell. Simul. Mater. Sci. Eng. **5**, 105 (1997).